# Morphological changes of Si in Al-Si alloys and a short fibre composite

F. Lasagni[1]*, H. P. Degischer[1], M. Papakyriacou[2]

[1] *Institute of Materials Science and Technology, Vienna University of Technology, Karlsplatz 13/E308 (A-1040), Vienna, Austria*
[2] *ARC Leichmetallkompetenzzentrum Ranshofen GmbH, (A-5282) Ranshofen, Austria*

Received 26 July 2005, received in revised form 2 March 2006, accepted 2 March 2006

**Abstract**

Thermal stability of Al-Si alloys and their composites is an important property for their application in engine components. In this work the thermal expansion and the physical Coefficient of Thermal Expansion (CTE) of AlSi1.1, -1.7, -7, -12 alloys and AlSi7/$Al_2O_3$/20s short fibre composite material are presented. The higher the Si content the more decreases the expansion of the alloys. Random planar alumina fibres reduce the in-plane thermal expansion, but the transverse expansion is significantly increased with respect to the matrix. The precipitation kinetics of Si is studied by means of Differential Scanning Calorimetry (DSC). Precipitation peaks correlate with an increase in the CTE of the alloys and the composite.

Al-Si alloys with 7 wt.% and higher content of Si present a percolating Si-network in the as-cast condition. The disintegration of this network during solutionizing results in a decrease of the hardness of the alloy. On the other hand, the hardness of the composite is increased during solution treatment via the formation of Si bridges between the short fibres, which strengthen the Si/$Al_2O_3$-network. The reinforcing networks' architecture is revealed by deep etching. It causes reversible viscous flow of the Al-matrix at temperatures > 300 °C.

K e y w o r d s: thermal expansion, Si precipitation, differential scanning calorimetry, hardness, spheroidization, Al-Si alloys, metal matrix composites

## 1. Introduction

Al-based alloys are used widely due to their light weight and high strength, compared with pure Al. Metal matrix composites are considered attractive choices for use in automotive engines because of the advantageous thermal and mechanical properties, such as enhanced specific strength and stiffness provided by the ceramic reinforcement and some ductility by the Al-alloys [1]. Particularly, the coefficient of thermal expansion is one of the important thermomechanical properties. The dimensional stability can be a critical issue for the service lifetime of engine components that are exposed to thermal cycling like pistons [2].

Thermal treatments of age hardening alloys like Al-Si containing Mg and/or Cu are to improve the mechanical properties appropriate for the final application. During solution treatment, the as-cast microstructure is reheated to below the eutectic temperature, which is appropriately termed during a time $t$. This process is followed by water quenching to maintain supersaturation, and can be followed by an ageing treatment at moderate temperature to produce a high density of small precipitates, increasing the hardness of the alloy. The Al-Si binary system is designated as non-age-hardening. The main reason for a solution treatment is not to dissolve the Si phase, the solubility of which is only 1.6 wt.% at the eutectic temperature (1.2 wt.% at 540 °C). Actually, the solution treatment of alloys containing more than 2 wt.% Si is a spheroidization treatment, the main objective of which is to improve the ductility of the eutectic material. After solution treatment, dimensional stabilization becomes important for hot parts in Al-engines, where local dimensional

*Corresponding author: tel.: +43 1 58801 30828; fax: +43 1 58801 30899; e-mail address: lasagni@pop.tuwien.ac.at

Table 1. Composition of the alloys (wt.%), rest Al

| Alloy | Si | Fe | Cu | Ni |
|---|---|---|---|---|
| AlSi1.1 | 1.11 | 0.0897 | 0.0029 | 0.0036 |
| AlSi1.7 | 1.74 | 0.0655 | 0.0024 | 0.0049 |
| AlSi7 | 7.04 | 0.0656 | 0.0024 | 0.0066 |
| AlSi12 | 11.87 | 0.0803 | 0.0023 | 0.0065 |

changes with exposure time would induce additional stresses.

Intensive work has been done in order to investigate the effect of Si spheroidization on microstructure and mechanical properties in Al-Si alloys [3, 4]. Aluminium alloys with 7 wt.% or higher content of Si show a percolating Si network in the as-cast condition, which disintegrates during solution treatment due to Si spheroidization [5]. In the present work, the spheroidization effect on the microstructure and hardness as well as the thermal expansion of Al-Si alloys and composite materials after different cooling rates from solution treatment temperature were studied.

## 2. Experimental procedures

### 2.1. Description of materials

Different Al-Si alloys and a composite material were produced using a squeeze casting process by LKR Ranshofen, Austria. A preform with randomly planar distributed short Saffil fibres (produced by Thermal Ceramics de France S. A.) was infiltrated with AlSi7 in order to obtain a 20 vol.% SFRM. Hereafter, the composite will be referred to as AlSi7/$Al_2O_3$/20s. The composition of the matrix and the unreinforced alloys is depicted in Table 1.

Figure 1a shows an optical micrograph of the as-cast SFRM looking onto the plane of random planar fibre orientation. A uniform distribution of the reinforcement can be observed. The microstructures of as-cast AlSi1.7 and AlSi7 alloys are depicted in Figures 1b and 1c, respectively. The AlSi1.7 material consists of an $\alpha$-aluminium phase (comparable to AlSi1.1) but with a small amount of eutectic Si phase along the grain boundaries. The $\alpha$-phase of AlSi7 is enclosed by the eutectic structure with lamellar Si, while AlSi12 is mostly eutectic.

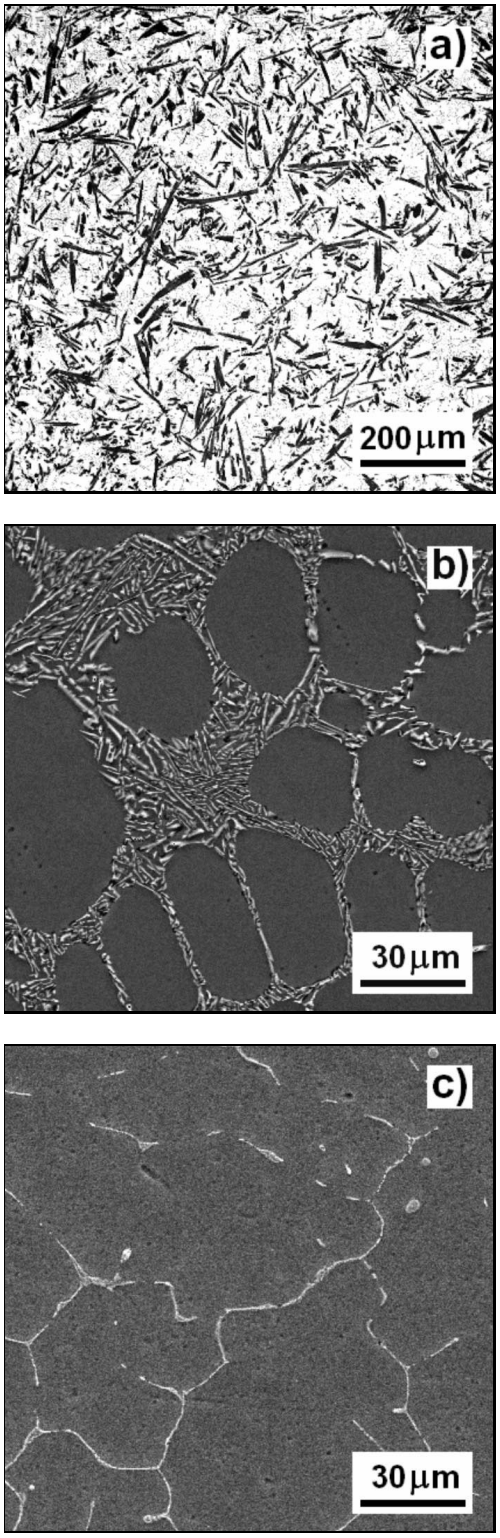


Fig. 1. Optical micrographs of a) AlSi7/$Al_2O_3$/20s looking onto the plane of random planar distribution of fibres, b) AlSi7 and c) AlSi1.7 as-cast.

### 2.2. Thermal expansion and DSC measurements

Samples of $15 \times 4 \times 2$ mm$^3$ size were cut in order to perform dilatometric measurements in a TMA (Thermomechanical Analyser) 2940 CE equipment from TA Instruments, Inc. Specimens of the composite material were cut with their longitudinal axes within the random fibre plane and in the perpendicular direc-

tion. Samples for dilatometry were solution treated (ST) at 540 °C during 15 min for the unreinforced alloys and 4 h for the SFRM, water quenched to T4 condition. Some specimens were subsequently heated again to 540 °C/15 min and cooled to room temperature at cooling rates of 20 or 1 K/min in the TMA device, which will be referred to as T4a and T4b conditions, respectively. After solution treatment, dilatometric tests were carried out where the expansion ($\Delta l$) of the specimens was measured between RT and 540 °C at a heating rate of 3 K/min in a nitrogen atmosphere. A numerical derivative of the $\Delta l$ vs. $T$-curve smoothed within intervals of $\pm 12.5$ K provides the instantaneous coefficient of thermal expansion (CTE) as $\alpha_T = (1/L) \cdot dL/dT$, where $L$ is the length of the specimen at the respective temperature.

DSC (Differential Scanning Calorimetry) runs of AlSi1.7 samples were carried out after T4 and T4a,b solution treatments in order to compare phase changes with the CTE. The measurements were performed in a DSC 2920 equipment using a heating rate of 5 K/min in nitrogen atmosphere.

### 2.3. Microstructural analysis of Si-$Al_2O_3$ structures – hardness tests

AlSi7/$Al_2O_3$/20s cubes of $10 \times 10 \times 10$ mm$^3$ size were solution treated at 540 °C during 20, 80 and 240 min and subsequently water quenched. Brinell hardness tests using a load of 10 kg and a 1 mm diameter ball were performed by means of an universal hardness tester model M1C010 provided by Emcotest. The $\alpha$-Al of the SFRM was dissolved using 17 wt.% of HCl solution until no more reaction bubbles were observed (approx. 24 h). Vickers hardness using a load of 0.1 kg was measured on the plane of randomly distributed fibres producing a contact area of about 0.6 mm$^2$ on the remaining Si/$Al_2O_3$ network structure extracted from specimens submitted to different solution treatment periods. The resulting Si/$Al_2O_3$ networks were observed by means of an FEI strata DB 235 electron microscope at Saarland University.

## 3. Results and discussion

### 3.1. Influence of Si precipitation on the thermal expansion

Figure 2a shows the thermal expansion of the different AlSi alloys and the composite material after a slow cooling at 1 K/min from solution treatment temperature (T4b). All these are reversible for dilatometric cycles at 3 K/min without remaining change in the specimens' length. The alloys expand more or less linearly, but at a lower rate with increasing Si content due to the lower CTE of Si (Si: 2.5–4 ppm/K, Al: 23–34 ppm/K between 25–530 °C [6]). The thermal expansion of AlSi1.1 T4b is close to that of pure Al. The addition of 12 wt.% Si reduces the linear expansion of Al from RT to 500 °C by 0.2 %.

The thermal expansion of AlSi1.7 after different cooling rates from the solution treatment, i.e. T4 and T4a,b, is depicted in Fig. 2b. The length of AlSi1.7 samples after slow cooling at 1 K/min from 540 °C increases as pure Al. By increasing the cooling rate after solution treatment to 20 K/min, a small deviation from pure Al for temperatures higher than 350 °C is observed. This deviation is considerably increased for the water quenched samples presenting an increment in the linear expansion of about 0.07–0.10 % with respect to pure Al or slowly cooled AlSi1.7 between 200–300 °C, producing a corresponding permanent length change. The permanent length change of the dilatometry samples in the different initial condition can be seen at the end of the dilatation curves in Fig. 2b at 540 °C. There, the length change of about 0.05 % can be read from the difference between the T4 test results and the reproducible curve obtained for the T4b condition. All dilatometric cycles at 3 K/min heating and cooling rate reproduce the T4b dilatation curves after the first similar cycle with any initial material condition.

DSC runs of water quenched AlSi1.7 samples show an exothermic peak between 200–300 °C (Fig. 3a-A) due to the formation of Si precipitates, which agrees with previous investigation [7]. Si dissolves in an fcc Al-cell during solution treatment which has an atomic volume of $6.60 \times 10^{-23}$ cm$^3$/at. Si precipitates by forming a diamond structure with an atomic volume 21 % higher ($8.01 \times 10^{-23}$ cm$^3$/at) than in fcc Al-Si. Therefore, Si precipitation causes an expansion of the alloys, which could reach 0.25 vol.%, if all 1.2 % Si dissolved at 540 °C could be quenched in and precipitated afterwards. A corresponding volume change of 0.2–0.3 vol.% is expected from the increment measured in linear expansion of the T4 condition from RT to 300 °C.

The exothermic peak (A) for T4 condition of about 0.015 W/g observed by DSC coincides with the CTE peak calculated from $\Delta l$ vs. $T$-curves (about 56 ppm/K). The precipitation peak is followed by an endothermic reversion up to the end of the measured temperature interval (Fig. 3a-B). This peak (B) at 510 °C is due to the dissolution of Si causing a reduction in the atomic volume to that of Al-fcc again. This is confirmed by the reduction of the CTE, which drops below that of pure Al.

Figure 3b depicts the coefficient of thermal expansion and heat flow vs. temperature of AlSi1.7 samples after slow cooling at 1 (T4b) and 20 K/min (T4a) from solution treatment temperature. T4a condition presents an exothermic peak at 420 °C (Fig. 3b-A) of about 0.006 W/g, whereas in T4b no exothermic form-

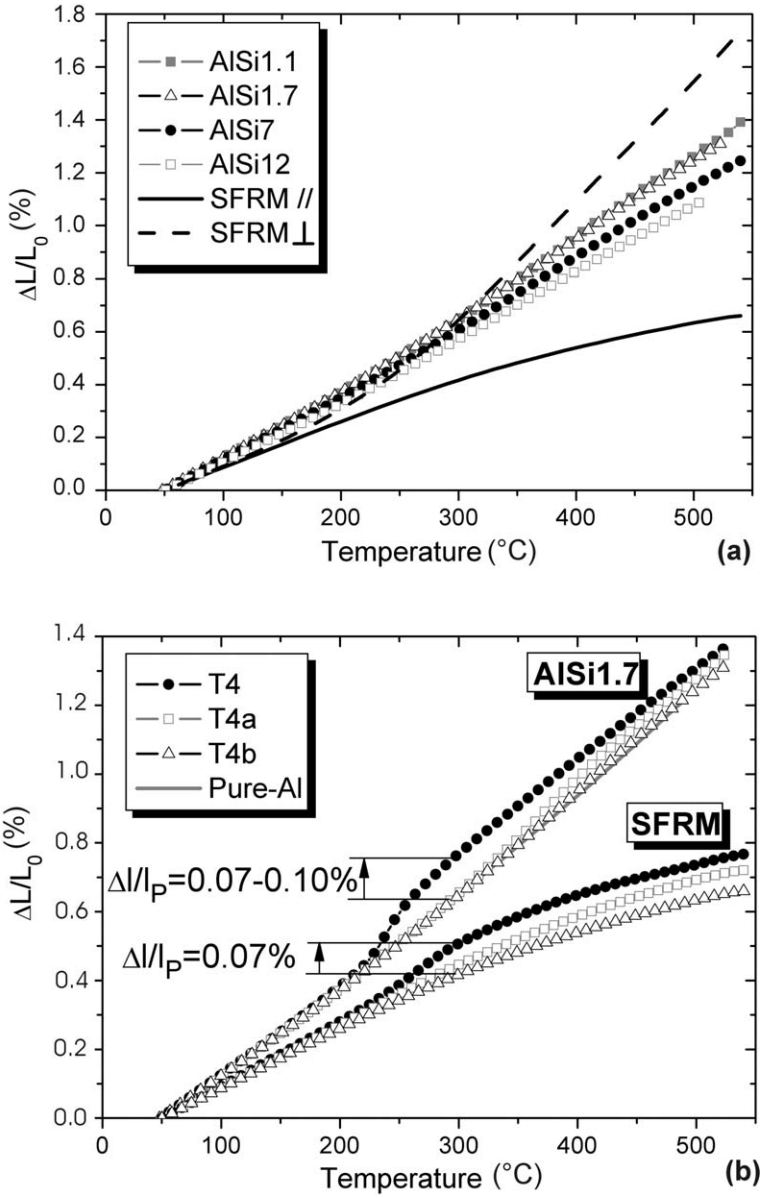


Fig. 2. Influence of a) Si content on the thermal expansion of Al-Si alloys and of fibre orientation in the SFRM (in-plane ∥ and transverse ⊥) after slow cooling (T4b = 1 K/min) from ST temperature, b) different cooling rates from ST on thermal expansion in AlSi1.7 and AlSi7/$Al_2O_3$/20s in fibre plane.

ation of Si precipitates was observed. This temperature range (A) agrees with the CTE peak for T4a, which amounts to 35 ppm/K. An endothermic peak (B) at about 510 ℃ was observed after the exothermic precipitation of Si (A) in the DSC curve for T4a condition. AlSi1.7 in T4b presents only an endothermic effect starting at lower temperatures (∼ 360 ℃). Both endothermic effects are related to the dissolution of Si causing a reduction in the measured CTE at the same temperature range, similar to the T4 condition. It can be noted that both the exothermic (A) and endothermic (B) peak shift considerably from lower to higher temperatures from the T4 to the T4a condition. The smaller the cooling rate the more Si precipitation takes place during cooling from ST. Therefore, less Si remains to precipitate during the following heating during dilatometric or DSC measurements producing less expansion and smaller precipitation peaks, respectively.

The CTE(T) curves AlSi7 submitted to different cooling rates from solution treatment temperature are depicted in Fig. 4a. The CTE of AlSi7 is smaller than that of AlSi1.7 for the whole temperature range, but shows similar precipitation peaks. A precipitation peak between 200–350 ℃ was observed after T4 solution treatment: somewhat smaller but shifted by 20 K to higher temperatures than for AlSi1.7. A precipitation peak of 30 ppm/K at 400 ℃ was observed after

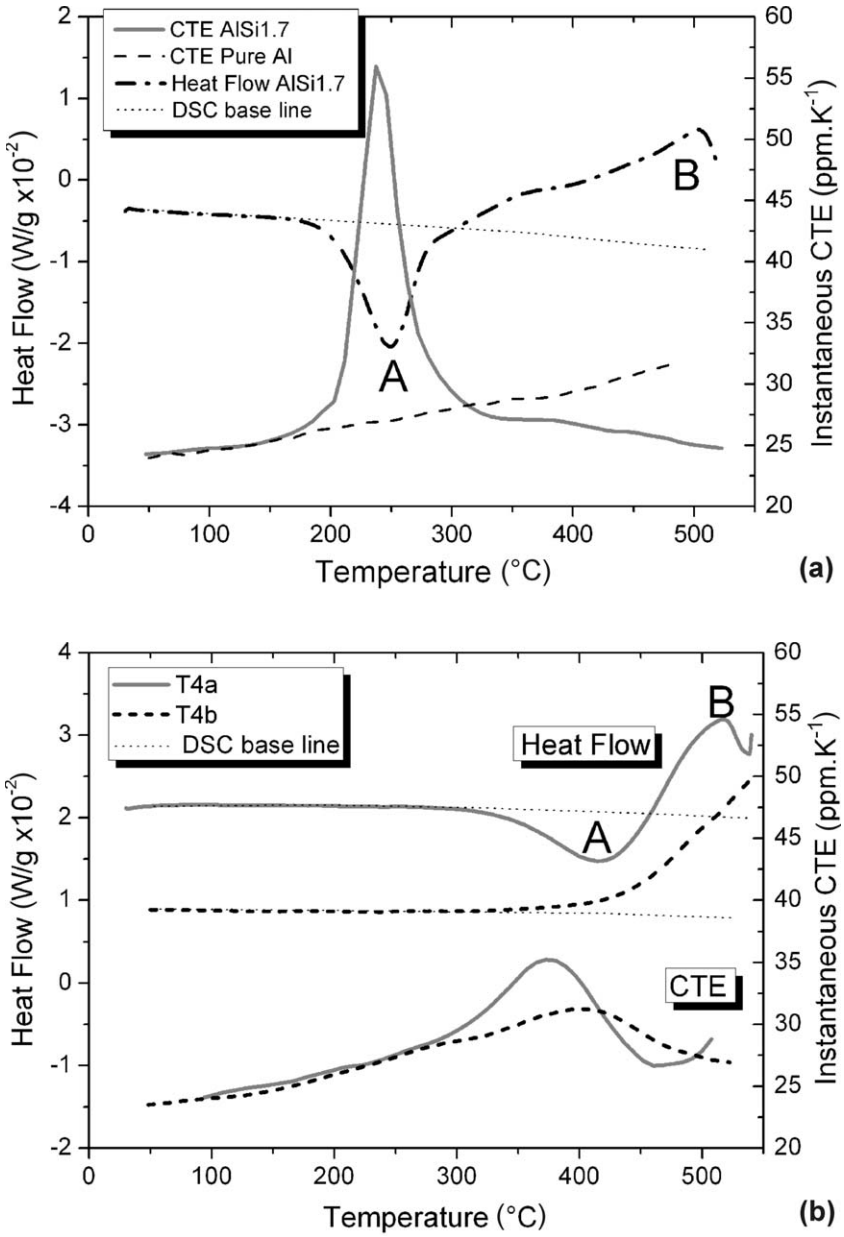


Fig. 3. Instantaneous CTE and DSC heat flow vs. temperature of AlSi1.7 in comparison with that of pure-Al after a) 4 h of ST at 540 °C + water quenching (T4) and b) 540 °C/4 h + slow cooling at 1 (T4b) and 20 K/min (T4a) to RT.

T4a, similarly to that of the slowly cooled AlSi1.7. The AlSi7 alloy behaves like an Al-matrix reinforced by 7 wt.% Si according to the thermoelastic models in the low temperature range. The CTE(T) curves of the AlSi7 alloy follow the elastic estimation by Schapery [8] only below 200 °C, when precipitation starts from T4 condition. This deviation begins at 300 °C for the T4a condition. The CTE curves drop below the thermoelastic prediction after the precipitation peak mainly due to re-dissolution of Si precipitates. The CTE(T) curve of AlSi7 in T4b condition follows the Schapery prediction until dissolution of Si precipitates starts at 400 °C. Yielding of the $\alpha$-Al is not expected in the unreinforced AlSi7 alloy during heating as the Si network is not percolating after ST. If matrix yielding occurred, the CTE(T) should raise above the elastic model independent of Si precipitation.

### 3.2. Influence of the short fibre reinforcement on thermal expansion

The thermal expansion of the composite (Fig. 2a) in the plane of fibre orientation is significantly below that of the matrix, but complementarily increasing in the transverse direction. 20 vol.% alumina fibres (5.5–7.9 ppm/K between RT – 500 °C [5]) in AlSi7 decrease significantly the in-plane expansion to half of that of

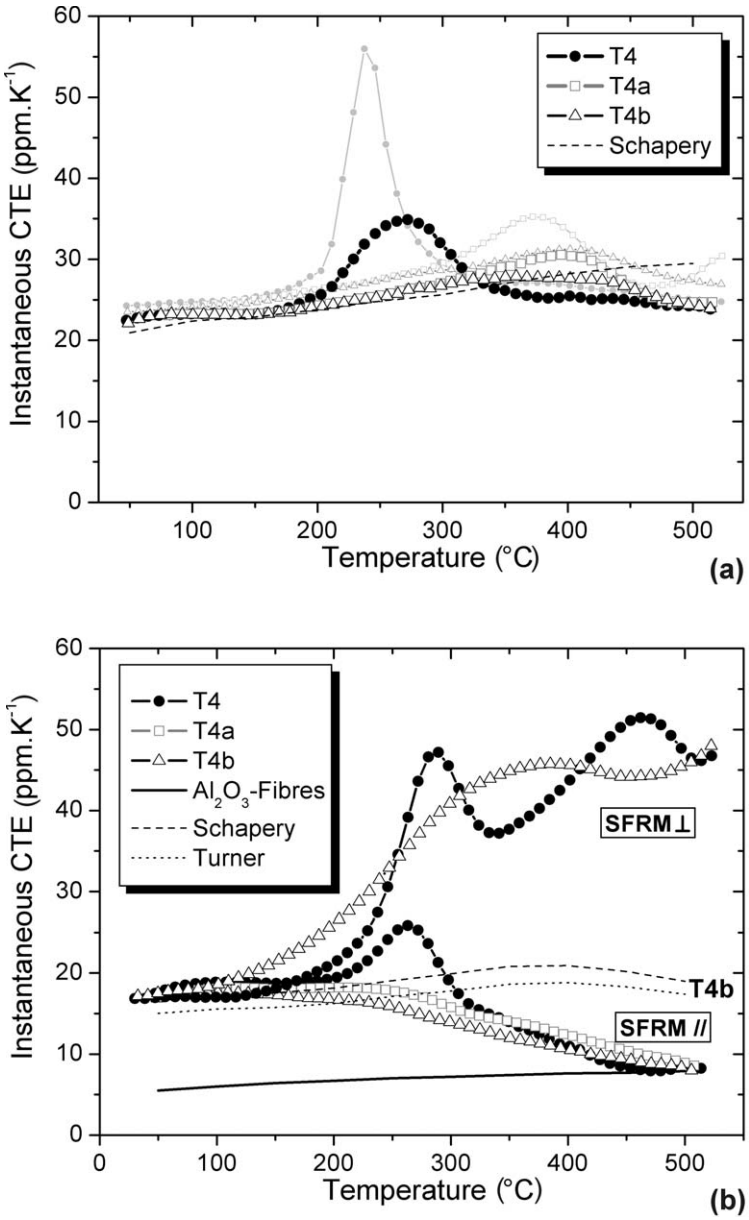


Fig. 4. Instantaneous CTE of a) AlSi1.7 T4 (light grey) and AlSi7 unreinforced matrix, and b) SFRM in fibre plane and perpendicular at different cooling rates from ST in comparison with elastic models.

AlSi7 from RT to 500 °C, whereas the transverse expansion increases by about 30 % with respect to the unreinforced matrix. The volume expansion of AlSi7 from RT to 540 °C amounts to 3.9 vol.% whereas that of the SFRM reaches only 3.1 vol.%. This means that the transverse expansion does roughly compensate the reduced in-plane expansion of the SFRM, if it is compared with the total expansion of the composite estimated by the rule of mixture: $0.8 \times 3.9$ vol.% + $0.2 \times 1$ vol.% = 3.3 vol.%.

The expansion of the T4b condition of all the alloys proceeds relatively linearly, while the expansion rate of the SFRM, i.e. the coefficient of thermal expansion, changes with temperature (see Fig. 2a). Figure 2b shows an additional expansion close to 300 °C increasing with the preceding cooling rate. The difference in the length change of the SFRM sample in the fibre plane between T4 and T4b condition up to 300 °C amounts to about 0.07 %, similar to that observed for the unreinforced alloy. The corresponding length change produced after the first heating of the SFRM in T4 condition in the dilatometer amounts to a linear shrinkage of about 0.15 % in the fibre plane compared with T4b. If dilatometric cycles are performed at 3 K/min heating and cooling rate, dilatation curves of any initial SFRM condition reproduce after the first cycle that of the stabilized T4b condition.

The CTE(T) curves of AlSi7/$Al_2O_3$/20s submit-

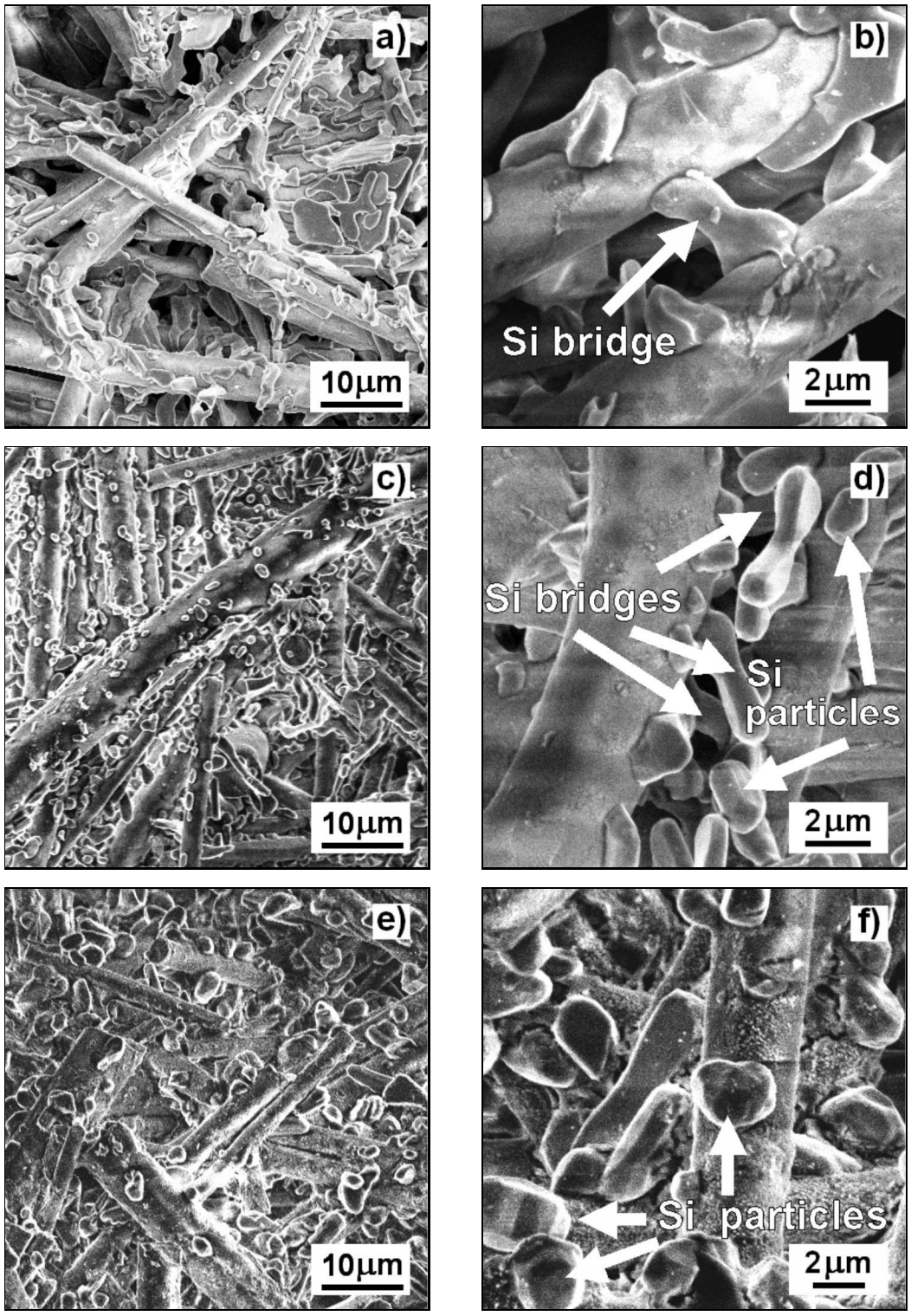


Fig. 5. $Si/Al_2O_3$ structure obtained after dissolution of the $\alpha$-Al for the $AlSi7/Al_2O_3/20s$ material in a), b) as-cast condition, c), d) after 20 min at 540 °C and e), f) after 4 h at 540 °C.

ted to different cooling rates from solution treatment temperature are depicted in Fig. 4b. The composite material in the fibre plane as well as transverse exhibits a precipitation peak in T4 condition between 200–320 °C. This effect disappears after slower cooling of 1 and 20 K/min from ST, which suggests that precipitation has been completed during slow cooling. The theoretical CTE of the SFRM was calculated according to the quoted thermoelastic models using the experimental CTE of the matrix according T4b and

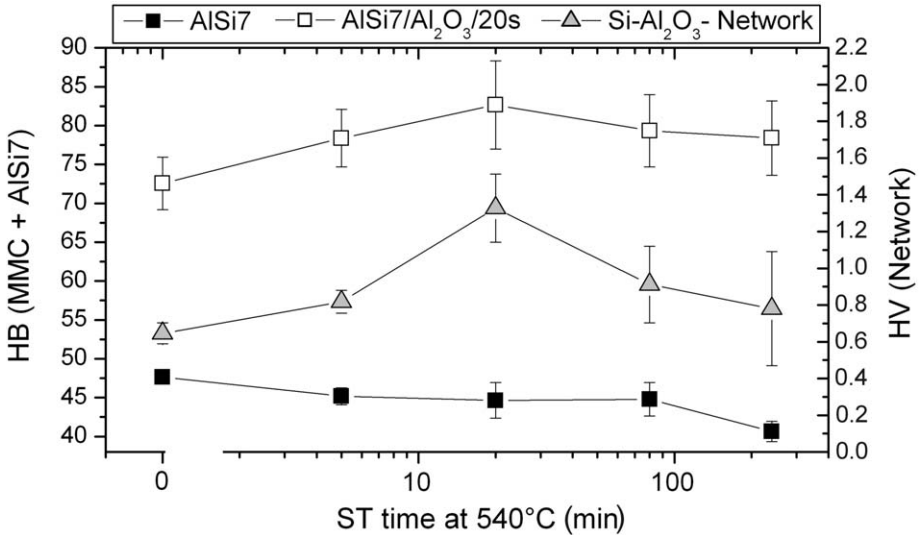


Fig. 6. Hardness test results for different solution treatment times by HB 1/10/10 for the AlSi7 alloy, AlSi7/$Al_2O_3$/20s composite and by HV 0.1/10 for the corresponding extracted Si/$Al_2O_3$ network.

that of $Al_2O_3$ from [5]. The experimental in-plane and transverse CTE of the SFRM follow the thermoelastic model reasonably well up to 200 ℃. In this temperature range tensile stresses build up in the matrix during cooling, which are relieved again during heating. The internal stresses produced by the mismatch between $Al_2O_3$-fibres and AlSi7 [8] invert from tension into compression during heating somewhere around 300 ℃, while the yield stress of the matrix drops facilitating relaxation. The viscoplastic deformation of the matrix causes the in-plane CTE to drop below the thermoelastic models according to Schapery and Turner [9] (the later assumes a percolating architecture of the $Al_2O_3$ phase). The CTE of the SFRM approaches that of alumina fibres, which is interpreted as a consequence of the percolating $Al_2O_3$-Si network. The reinforcement compresses the expanding Al matrix in the fibre plane at temperatures > 250 ℃, which may creep into the transverse direction and into pre-existing pores. The later was observed for Al/SiC/70p composites [10].

### 3.3. Influence of Si spheroidization on the rigidity of AlSi7/$Al_2O_3$/20s

Figure 5 shows SEM micrographs of the structures obtained after dissolution of the $\alpha$-Al from AlSi7/$Al_2O_3$/20s in the as-cast condition (Figs. 5a,b), solution treated during 20 min (Figs. 5c,d) and 4 h (Figs. 5e,f). The addition of the $Al_2O_3$ short fibres has inhibited the disintegration of the three-dimensional network within the matrix, which takes place rapidly for hypoeutectic Al-Si alloys [11]. The result is a Si/$Al_2O_3$ structure [12], which is stable for all the studied thermal conditions. Thin Si plates from the eutectic structure were observed in the as-cast condition bridging the fibres (Fig. 5a). During solution treatment, Si coarsens at $Al_2O_3$ fibres (Figs. 5c,d).

By increasing the solution treatment time to 4 h, many of the Si bridges have coalesced into individual Si particles located on the surface of the ceramic fibres. All these changes may affect the mechanical resistance of the network and hence of the composite. This is confirmed by the results of the hardness tests shown in Fig. 6, where the results for the AlSi7 matrix, the AlSi7/$Al_2O_3$/20s composite and the Si/$Al_2O_3$ network are displayed as a function of solution treatment time. A continuous decrease of the hardness by approximately 15 % takes place for the unreinforced matrix with increasing the solution treatment time up to 4 h. Contrarily to the matrix, the composite presents an increase of the hardness with a small peak at 20 min of solution treatment time. This is in qualitative agreement with the results obtained for the Si/$Al_2O_3$ network where a maximum is also observed at the same ST time. Thus, the spheroidization of the Si affects the resistance of the Si/$Al_2O_3$ network and is responsible for the "peak hardening" effect observed for the SFRM after 20 min ST at 540 ℃ (this observation would be confirmed by means of tensile tests, actually in progress). The same effect was observed for similar composite materials at a lower temperature (300 ℃) but after longer exposure times [11].

## 4. Conclusions

Fast quenching of Al-Si alloys causes Si-supersaturation. Slow heating causes an additional linear expansion (compared with pure Al) of about 0.07–0.1 %, i.e. 0.2–0.3 vol.%, for water quenched alloys and composite material due to Si precipitation. The pre-

cipitation peak observed in both CTE and DSC curves moves from 250 ℃ in T4 to 420 ℃ for slower cooled alloys. The retardation of Si precipitation may be correlated to reduced diffusivity with respect to the T4 condition, where supersaturation of vacancies is expected. The expansion of the materials due to Si-precipitation decreases after slow cooling (1–20 K/min) from solution treatment temperature, compared with the water quenched condition. CTE measurements for the composite material did not show any precipitation peaks for the T4a,b conditions, which is probably due to stable incoherent Si precipitation already during slow cooling. The addition of short fibres to AlSi7 may accelerate precipitation by introducing heterogeneous nuclei and easy interface diffusion paths.

The combination of $Al_2O_3$ short fibres and Al-Si alloys with more than 7 wt.% Si results in the formation of a three-dimensional $Si/Al_2O_3$ structure. Si spheroidization affects the rigidity of the $Si/Al_2O_3$ structure forming Si bridges connecting the ceramic fibres. While the unreinforced alloys loose in hardness due to spheroidization of the eutectic Si, the SFRM exhibits a temporary hardening effect. This percolating network reduces the CTE of the composite in the plane of fibre orientation, but not transversally. Above 300 ℃ the in-plane CTE approaches that of the reinforcement, while the transverse CTE remains constant at a level of almost twice the CTE of the matrix. The volume expansion of the SFRM is smaller than that estimated by the rule of mixtures. As the dilatometric curves after slow cooling are reproducible, this can be explained by reversible matrix creep activated by the elastic expansion of the reinforcement network.

## Acknowledgements

The present work was partly financed by the Austrian Non Kplus-programme via LKR. F. Lasagni would like to thank the ADEMAT Network (EU-Alfa II Programme) for the financial mobility support. The authors would also thank Prof. F. Mücklich and A. Lasagni of the Saarland University for SEM investigation.

## References

[1] KELLY, A.—ZWEBEN, C.: Comprehensive Composite Materials. Vol. 3. Amsterdam, Elsevier 2000.
[2] HENNING, W.—NIETE, G.—SCHMID, E.: Metall, *48*, 1994, p. 451.
[3] HAQUE, M. M.: J. Mater. Pro. Tech., *55*, 1995, p. 193.
[4] GUIGLIONDA, G.—POOLE, W. J.: Mater. Sci. and Eng., *A336*, 2002, p. 159.
[5] LASAGNI, F.—REQUENA, G.—DEGISCHER, H. P.—MINGLER, B.—PAPAKYRIACOUR, M.: In: Proceedings Metallographie Tagung. Eds.: Pohl M., Petzow, G. Vol. 36. Bochum, Werkstoff-Informationsgesellschaft GmbH 2004, p. 443.
[6] SHACKELFORD, J.—ALEXANDER, W.—PARK, J. S.: CRC Materials Science and Engineering Handbook, Boca Raton, Florida, CRC Press Inc. 1994.
[7] HÄLLDAHL, L.: Thermochimica Acta, *214*, 1993, p. 33.
[8] NASSINI, H. E.—MORENO, M.—OLIVER, G.: J. Mater. Sci., *36*, 2001, p. 2759.
[9] SCHAPERY, R. A.: J. Comp. Mat., *2*, 1968, p. 380.
[10] HUBER, T.—DEGISCHER, H. P.—LEFRANC, G.—SCHMITT, T.: Comp. Sci. & Techn., 2006, No. 3205 (in print).
[11] LASAGNI, F.—REQUENA, G.—DEGISCHER, H. P.—PAPAKYRIACOU, M.: In: Proceedings Verbundwerkstoffe. Eds.: Schlimmer, M., Kassel, Werkstoff-Informationsgesellschaft GmbH 2005, p. 57.
[12] CSEH, G.—BÄR, J.—GUDLADT, H.-J.—LENDVAI, J.—JUHÁSZ, A.: Mater. Sci. Eng., *A272*, 1999, p. 145.